Numer. Math. Theor. Meth. Appl.
doi: 10.4208/nmtma.2017.m1613

Vol. **10**, No. 1, pp. 186-204
February 2017

Total Variation Based Parameter-Free Model for Impulse Noise Removal

Federica Sciacchitano*, Yiqiu Dong and Martin S. Andersen

Department of Applied Mathematics and Computer Science,
Technical University of Denmark, 2800 Kgs. Lyngby, Denmark.

Received 14 March 2016; Accepted 13 June 2016

Abstract. We propose a new two-phase method for reconstruction of blurred images corrupted by impulse noise. In the first phase, we use a noise detector to identify the pixels that are contaminated by noise, and then, in the second phase, we reconstruct the noisy pixels by solving an equality constrained total variation minimization problem that preserves the exact values of the noise-free pixels. For images that are only corrupted by impulse noise (i.e., not blurred) we apply the semismooth Newton's method to a reduced problem, and if the images are also blurred, we solve the equality constrained reconstruction problem using a first-order primal-dual algorithm. The proposed model improves the computational efficiency (in the denoising case) and has the advantage of being regularization parameter-free. Our numerical results suggest that the method is competitive in terms of its restoration capabilities with respect to the other two-phase methods.

AMS subject classifications: 68U10, 94A08, 49J40, 52A41, 65K10, 90C47, 49M15

Key words: Image deblurring, image denoising, impulse noise, noise detector, primal-dual first-order algorithm, semismooth Newton method, total variation regularization.

1. Introduction

During the image acquisition and transmission, observed images are inevitably degraded by blur and noise. In the literature, many kinds of noise have been widely considered, Gaussian noise [14,20,36], impulse noise [7,11,28,29,31], multiplicative noise [3, 19, 35], Poisson noise [21, 26, 37] or mixed noise [8, 27, 38]. In this paper, we focus on blurred image with impulse noise, which is a common type of image degradation due to, e.g., malfunctioning pixel elements in the camera sensors, errors in analog-to-digital conversion, faulty memory locations in hardware, or transmission errors [5]. A characteristic property of impulse noise is that a certain number of pixels

*Corresponding author. *Email addresses:* feds@dtu.dk (F. Sciacchitano), yido@dtu.dk (Y. Dong), mskan@dtu.dk (M. S. Andersen)

 ©2017 Global-Science Press

https://doi.org/10.4208/nmtma.2017.m1613 Published online by Cambridge University Press

are uncorrupted and the noise-corrupted pixels contain no information about the true pixel value.

Over the years, many nonlinear digital filters methods have been proposed, see [2]. The most common filters used to remove impulse noise are the median-type filters: median filter [34], weighted median filter [6], adaptive median filter [24], multistate median filter [15], center weighted median filter [25] and adaptive center-weighted median filter [16]. Although these filters are efficient and easy to implement, they cannot achieve good results in general, in particular they are not able to restore a blurred image and they do not preserve the image edges well.

In order to preserve the edges, in 2004, Nikolova [31] proposed a variational model which combines an ℓ^1-data fidelity term with total variation (TV), which has been in shown in [30, 31] to work better than the classical ℓ^2-term, [36].

Later, other approaches based on the ℓ^1-TV have been proposed to handle the deblurring problem and the non-differentiability of the ℓ^1-norm, for instance: Bar *et al.* [4] introduce a model using the Mumford-Shah regularizer and the ℓ^1-data fidelity term; Yang *et al.* [39] suggested an efficient algorithm to solve the ℓ^1-TV model; Dong *et al.* [17] solved the ℓ^1-TV model using a primal-dual approach.

However, since the ℓ^1-TV minimization method negatively affects the noisy-free pixels, in 2005, Chan, Ho, and Nikolova [12] proposed the so-called two-phase method. The basic idea behind this method, which we will refer to as the CHN method, is to separate noise detection and image reconstruction. In the first phase, the method uses a noise detector to identify which pixels are corrupted, and in the second phase, it reconstructs only the noisy pixels based on an objective function with an ℓ^1-data fidelity term and with TV as a regularization term. The two-phase model has also been studied for other applications, for instance in [8], the authors apply the two-phase method to restore blurred images with impulse and Gaussian noise; in [23], a two-phase method is used for recovering images corrupted by multiplicative noise; in [7] and [11], a two-phase method is used to simultaneously deblur and denoise an image with impulse noise. Different from [12], in the second phase of [7] and [11] the authors reconstruct the image based on a modified ℓ^1-TV model where only noise-free pixels are kept in the ℓ^1-data fidelity term, due to no useful information contained in impulse noise. We will focus only on the method in [11] (the CDH method in short), since it outperforms the one in [7] and [12] with respect to both image restoration capability and computational efficiency.

While the CDH method has been shown to perform well on many test problems, the inclusion of noise-free pixels in the data-fidelity term is somewhat at odds with the assumption that their true values are known. If the pixels are indeed noise-free, then they can either be treated as constants or eliminated from the problem. In this work, we investigate such an approach and propose a modified two-phase method. In particular, as suggested in [11], in the first phase we distinguish noisy pixels from the noise-free pixels by the adaptive median (AM) filter [24] for detecting salt-and-pepper noise, and the adaptive center-weighted median (ACWM) filter [16] for random-valued impulse noise. The detector for salt-and-pepper noise is able to detect almost all noisy

https://doi.org/10.4208/nmtma.2017.m1613 Published online by Cambridge University Press

pixels even for noise level around 90%, while for random-valued impulse noise, the ACWM works quite well until a noise level of 40%, since in this case the noisy pixels can be confused as clean ones and vice-versa. In case of higher noise for random-valued impulse noise, we suggest to use other filters, e.g. [1] and [18], which have the capability to detect noisy pixels in images with noise percentage up to 60%. The study of a good detector for random-valued impulse nose is outside the scope of this paper.

In the second phase, we compute the reconstruction by solving a reduced TV minimization problem that involves only the corrupted pixels. For solving the problem, we employ the semismooth Newton method, [32]. Furthermore, if the noise level is below 30%, we speed up the process by preprocessing the independent noisy pixels. The main difference between our method and the CDH method is that we reconstruct only the pixels that are identified as corrupted by noise instead of all pixels. For this reason, our method often leads to computational savings, and it can be viewed as an exact method in the sense that the reconstruction model matches the information about the noise-free pixels. Moreover, a notable advantage of our model is that the reconstruction results do not rely on the adjustment of any regularization parameters.

In addition to the impulse noise denoising problem, we also consider simultaneous deblurring and denoising. Instead of including the noise-free pixels in a data-fidelity term, we propose a regularization parameter-free model based on a constrained minimization problem. We solve this problem numerically using a primal-dual first-order algorithm [10].

This study focuses on the second phase of the two-phase method, and the main contributions regard the introduction of a regularization parameter-free model to reconstruct the corrupted image and, for the denoising case, the computational efficiency compared to the latest two-phase method, especially given by the preprocessing part.

The paper is organized as follows. In Section 2, we review the impulse noise model and propose a two-phase methods for denoising and also deblurring images. In Section 3, we present the implementation details, and in Section 4, we show some numerical results. We conclude the paper in Section 5.

2. The regularization parameter-free two-phase models

We start this section by introducing two impulse noise models, namely salt-and-pepper noise and random-valued impulse noise. Then, inspired by the existing denoising models in the literature [11], we propose (i) a two-phase method for denoising, and (ii) a two-phase method for simultaneous denoising and deblurring.

Given a discrete image of size $m_1 \times m_2$, we define a vector $\boldsymbol{u} \in \mathbb{R}^m$ with the $m = m_1 m_2$ pixels. We shall use the following notation $u_k = u_{i,j}$, where $k = (i-1)m_2 + j$ for $i = 1, \dots, m_1$ and $j = 1, \dots, m_2$, to identify the pixel at position (i, j) with the kth element of $\boldsymbol{u}$, and we define a set $\Omega = \{1, 2, \dots, m\}$ that contains all pixel indices.

https://doi.org/10.4208/nmtma.2017.m1613 Published online by Cambridge University Press

2.1. Impulse noise models

Impulse noise can be described as a stochastic degradation process of the form

$$z_k = N_r(\tilde{u}_k) = \begin{cases} \eta_k & \text{with probability } r, \\ \tilde{u}_k & \text{with probability } 1-r, \end{cases} \qquad k \in \Omega,$$

where $\tilde{\boldsymbol{u}} \in \mathbb{R}^m$ is the original image, $\boldsymbol{z} \in \mathbb{R}^m$ is the corrupted image, and $\boldsymbol{\eta} \in \mathbb{R}^m$ is the noise, which is independent from the original image $\tilde{\boldsymbol{u}}$. Both images are assumed to be obtained from a two-dimensional pixel-array by means of columnwise concatenation. We refer to the parameter $r \in [0,1]$ as the noise level since it can be interpreted as the probability that a pixel is corrupted. Notice that some pixels remain unchanged, and the pixels that are corrupted by noise carry no information about the noise-free image.

Two main types of impulse noise are the salt-and-pepper noise when, for each k, the noise η_k is a discrete random variable with values drawn from the set $\{d_{\min}, d_{\max}\}$ with equal probability (with $d_{\min} = \min_k \tilde{u}_k$ and $d_{\max} = \max_k \tilde{u}_k$), and the random-valued impulse noise when, for each k, the noise η_k is a uniformly distributed random variable with values in the gray-level range $[d_{\min}, d_{\max}]$. For salt-and-pepper noise corrupted pixels take the lowest or the highest pixel value (i.e., $d_{\min}$ or $d_{\max}$), whereas for random-valued impulse noise, the noisy pixels have values anywhere in the interval from $d_{\min}$ to $d_{\max}$. Then, the random-valued impulse noise is more general and more difficult to detect than the salt-and-pepper noise.

2.2. Denoising models

The ℓ^1-TV model for impulse noise denoising proposed by Nikolova [30, 31] combines the TV regularization term with an ℓ^1 data-fidelity term. The resulting reconstruction problem is convex and takes the following form

$$\min_{\boldsymbol{u} \in \mathbb{R}^m} \|\boldsymbol{u} - \boldsymbol{z}\|_1 + \alpha \, \mathrm{TV}(\boldsymbol{u}), \tag{2.1}$$

where $\|\boldsymbol{u} - \boldsymbol{z}\|_1 = \sum_{k \in \Omega} |u_k - z_k|$ is the data-fidelity term, $\mathrm{TV}(\boldsymbol{u})$ is a regularization term, and $\alpha > 0$ is a regularization parameter. The (discrete) TV is defined as

$$\mathrm{TV}(\boldsymbol{u}) := \sum_{k \in \Omega} |(\nabla \boldsymbol{u})_k|_2 = \sum_{k \in \Omega} \sqrt{|(\nabla_x \boldsymbol{u})_k|^2 + |(\nabla_y \boldsymbol{u})_k|^2},$$

where the discrete gradient operator $\nabla \in \mathbb{R}^{2m \times m}$ is given by

$$(\nabla \boldsymbol{u})_k = \begin{pmatrix} (\nabla_x \boldsymbol{u})_k \\ (\nabla_y \boldsymbol{u})_k \end{pmatrix},$$

and $\nabla_x \boldsymbol{u}$ and $\nabla_y \boldsymbol{u}$ denote the horizontal and vertical first order differences, i.e., using the symmetric boundary conditions, we have

$$(\nabla_x \boldsymbol{u})_k = \begin{cases} u_{i+1,j} - u_{i,j} & \text{if } i < m_1, \\ 0 & \text{if } i = m_1, \end{cases} \quad \text{and} \quad (\nabla_y \boldsymbol{u})_k = \begin{cases} u_{i,j+1} - u_{i,j} & \text{if } j < m_2, \\ 0 & \text{if } j = m_2, \end{cases}$$

https://doi.org/10.4208/nmtma.2017.m1613 Published online by Cambridge University Press

for $k = (i-1)m_2 + j$ with $i = 1, \dots, m_1$ and $j = 1, \dots, m_2$.

The ℓ^1-TV model has some nice properties, such as contrast preservation, multiscale decomposition and morphological invariance [13, 30, 40]. However, as mentioned in the introduction, the main disadvantage of this approach is that we have to reconstruct all the pixels of the image, including the ones that are noise-free. Furthermore, including the noisy pixels in the data-fidelity term introduces errors since the noise-corrupted pixels contain no information about the true image. To address this issue, Chan *et al.* [11] studied a two-phase method (the CDH method) in which they first detect the noisy pixels (phase 1) and then exclude these pixels from the data-fidelity term when computing a reconstruction (phase 2). Thus, in the first phase, they use a detector (an AM filter for salt-and-pepper and an ACWM filter for random-valued impulse noise) to split the domain Ω into two sets: $\mathcal{N}$ that includes all indices of the corrupted pixels and $\mathcal{U}$ that includes the indices of the noise-free pixels. We will henceforth assume that there are $|\mathcal{N}| = n$ noisy pixels and $|\mathcal{U}| = m - n$ noise-free pixels. In the second phase, for the denoising case (here, instead of the blurring operator we consider the identity), they reconstruct the image based on the following model

$$\min_{\boldsymbol{u} \in \mathbb{R}^m} \sum_{k \in \mathcal{U}} |u_k - z_k| + \alpha \, \mathrm{TV}(\boldsymbol{u}). \tag{2.2}$$

The main advantage of the CDH method is that the noise detector improves the data-fidelity term in ℓ^1-TV model (2.1), and this often yields a great improvement in terms of restoration capabilities. Furthermore, the ℓ^1-norm in the data-fidelity term allows many noisy-free pixels to maintain their exact values. However, the presence of a regularization parameter in the model necessitates multiple reconstructions or tests in order to find a good choice for the parameter. Moreover, the problem (2.2) includes all pixels of the image as variables, including the ones that are assumed to be free of noise. To overcome these disadvantages of the CDH method, we propose to alter the second phase of the method such that the noise-free pixels are required to be equal to their known values, i.e., we consider the following constrained optimization problem

$$\begin{aligned} &\min_{\boldsymbol{u} \in \mathbb{R}^m} \mathrm{TV}(\boldsymbol{u}) \\ &\text{s.t.} \quad u_k = z_k \quad k \in \mathcal{U}. \end{aligned} \tag{2.3}$$

In other words, instead of looking at the unconstrained minimization problem in (2.2), we are considering the constrained version of it. The equality constraints in this model reflect the exact prior that some pixels are known, assuming that all pixels were correctly identified as either noise-free or corrupted in the first phase. For this reason, the reconstruction model (2.2) can be seen as an approximation model since it allows the noise-free pixels to deviate from their known value.

Although the model (2.3) does not require the determination of any regularization parameters, it can be shown to be equivalent to (2.2) if the regularization parameter α is chosen sufficiently small. Specifically, we refer the reader to [32, Thm. 17.3] (note that, this theorem holds in the continuous case).

https://doi.org/10.4208/nmtma.2017.m1613 Published online by Cambridge University Press

Unlike the model (2.2), which includes all pixels as variables, the constrained problem (2.3) allows us to eliminate the variables that correspond to noise-free pixels from the problem formulation. To write (2.3) as an unconstrained optimization problem, we define a vector $\boldsymbol{u}_{\mathcal{N}} \in \mathbb{R}^n$ that corresponds to the corrupted pixels. With this notation, $\boldsymbol{u}$ can be expressed as

$$\boldsymbol{u} = \Lambda_{\mathcal{N}} \boldsymbol{u}_{\mathcal{N}} + \Lambda_{\mathcal{U}} \boldsymbol{u}, \tag{2.4}$$

where $\Lambda_{\mathcal{U}} \in \mathbb{R}^{m \times m}$ is a diagonal matrix defined as

$$(\Lambda_{\mathcal{U}})_{i,i} = \begin{cases} 1 & \text{if } i \in \mathcal{U} \\ 0 & \text{if } i \in \mathcal{N} \end{cases}$$

and $\Lambda_{\mathcal{N}} \in \mathbb{R}^{m \times n}$ is a matrix with n unit vectors $\boldsymbol{e}_j \in \mathbb{R}^m$, $j \in \mathcal{N}$, as columns. Note that $\Lambda_{\mathcal{U}} \Lambda_{\mathcal{N}} = 0$ by construction. Since $\Lambda_{\mathcal{U}} \boldsymbol{u}$ represents the intensity of the noise-free pixels, based on the constraint in (2.3), we can substitute $\Lambda_{\mathcal{U}} \boldsymbol{z}$ into (2.4) and express the image $\boldsymbol{u}$ as follows

$$\boldsymbol{u} = \Lambda_{\mathcal{N}} \boldsymbol{u}_{\mathcal{N}} + \Lambda_{\mathcal{U}} \boldsymbol{z}. \tag{2.5}$$

The problem (2.3) can therefore be expressed in terms of $\boldsymbol{u}_{\mathcal{N}}$ as follows

$$\min_{\boldsymbol{u}_{\mathcal{N}} \in \mathbb{R}^n} \mathrm{TV}(\Lambda_{\mathcal{N}} \boldsymbol{u}_{\mathcal{N}} + \Lambda_{\mathcal{U}} \boldsymbol{z}). \tag{2.6}$$

Comparing this model with (2.2), we see that both are unconstrained minimization problems, but (2.6) has some advantages. Firstly, the minimization problem involves only n variables instead of m variables, and if the noise level is relatively low (i.e. $n \ll m$) the reduction in the number of variables is quite substantial. Secondly, it does not require the determination of the regularization parameter.

Before we discuss how to solve (2.6), we first consider an extension of our denoising approach to simultaneous deblurring and denoising.

2.3. Deblurring and denoising models

Suppose the observed image $\boldsymbol{z}$ is not only corrupted by impulse noise but also blurred by a known linear blur operator $K \in \mathbb{R}^{m \times m}$, i.e., we define $\boldsymbol{z} = N_r(K\boldsymbol{u})$. To solve the deblurring and denoising problem, we consider the two-phase method in [11], which extends the CHN method for the general case. In the first phase, the authors of [11] identify the corrupted pixels, and then, in the second phase, they compute a reconstruction by solving the following problem

$$\min_{\boldsymbol{u} \in \mathbb{R}^m} \sum_{k \in \mathcal{U}} |(K\boldsymbol{u})_k - z_k| + \alpha \, \mathrm{TV}(\boldsymbol{u}). \tag{2.7}$$

Note that only the noise-free pixels are included in the data-fidelity term. As in the denoising problem (2.3), we can formulate a constrained minimization problem

$$\begin{aligned} &\min_{\boldsymbol{u} \in \mathbb{R}^m} \mathrm{TV}(\boldsymbol{u}) \\ &\text{s.t.} \quad (K\boldsymbol{u})_k = z_k \quad k \in \mathcal{U} \end{aligned} \tag{2.8}$$

https://doi.org/10.4208/nmtma.2017.m1613 Published online by Cambridge University Press

which implies that the value of noise-free pixels in the blurred image are treated as known constants. However, unlike in the denoising case, the blur operator K introduces coupling and makes it difficult to eliminate the equality constraints. In the next section, we address how to solve the problem numerically.

3. The algorithms

We now present methods for solving the denoising problem (2.6) as well as the deblurring and denoising problem (2.8).

3.1. Solving the denoising problem

Since the objective function in (2.6) is not differentiable everywhere, we introduce the following smooth approximation of TV,

$$\mathrm{TV}^\gamma(\boldsymbol{u}) = \sum_{k\in\Omega} \Phi^\gamma(|(\nabla \boldsymbol{u})_k|_2),$$

where the function Φ^γ is the Huber function which is defined as

$$\Phi^\gamma(t) = \begin{cases} |t| - \frac{\gamma}{2} & \text{if } |t| \geq \gamma \\ \frac{1}{2\gamma}|t|^2 & \text{else,} \end{cases}$$

with parameter $\gamma > 0$. Other smooth approximations may be used instead, such as e.g. $\sqrt{t^2+\gamma^2}$. The gradient of $\mathrm{TV}^\gamma(\Lambda_\mathcal{N}\boldsymbol{u}_\mathcal{N} + \Lambda_\mathcal{U}\boldsymbol{z})$ can be expressed as

$$F^\gamma(\boldsymbol{u}_\mathcal{N}) = -\Lambda_\mathcal{N}^\top \mathrm{div}\, \mathcal{D}^\gamma(\boldsymbol{u}_\mathcal{N})^{-1} \nabla(\Lambda_\mathcal{N}\boldsymbol{u}_\mathcal{N} + \Lambda_\mathcal{U}\boldsymbol{z}),$$

where $\mathrm{div} \in \mathbb{R}^{m\times 2m}$ represents the divergence, $\mathcal{D}^\gamma(\boldsymbol{u}_\mathcal{N}) \in \mathbb{R}^{2m\times 2m}$ is defined as

$$\mathcal{D}^\gamma(\boldsymbol{u}_\mathcal{N}) = \begin{pmatrix} N^\gamma(\boldsymbol{u}_\mathcal{N}) & 0 \\ 0 & N^\gamma(\boldsymbol{u}_\mathcal{N}) \end{pmatrix},$$

and $N^\gamma(\boldsymbol{u}_\mathcal{N}) \in \mathbb{R}^{m\times m}$ is a diagonal matrix with diagonal $\max\big(|\nabla(\Lambda_\mathcal{N}\boldsymbol{u}_\mathcal{N} + \Lambda_\mathcal{U}\boldsymbol{z})|_2, \gamma\big)$. The divergence satisfies the equation $\mathrm{div} = -\nabla^\top$, where $\nabla^\top$ is the transpose of the gradient operator. Hence, the explicit formula of the divergence can be found using the definition of transpose

$$\langle -\mathrm{div}\, \boldsymbol{p}, \boldsymbol{v}\rangle_{\mathbb{R}^m} = \langle \boldsymbol{p}, \nabla \boldsymbol{v}\rangle_{\mathbb{R}^{2m}},$$

for every $\boldsymbol{p} \in \mathbb{R}^{2m}$ and $\boldsymbol{v} \in \mathbb{R}^m$, where $\langle\cdot,\cdot\rangle_{\mathbb{R}^m}$ and $\langle\cdot,\cdot\rangle_{\mathbb{R}^{2m}}$ denote the standard scalar products in $\mathbb{R}^m$ and $\mathbb{R}^{2m}$, respectively.

It follows from the first-order optimality condition associated with (2.6) that the solution to the smooth approximation should satisfy the following equation

$$\Lambda_\mathcal{N}^\top \mathrm{div}\, \mathcal{D}^\gamma(\boldsymbol{u}_\mathcal{N})^{-1} \nabla(\Lambda_\mathcal{N}\boldsymbol{u}_\mathcal{N} + \Lambda_\mathcal{U}\boldsymbol{z}) = 0. \tag{3.1}$$

https://doi.org/10.4208/nmtma.2017.m1613 Published online by Cambridge University Press

The nonlinear equation in (3.1) can be solved by the semismooth Newton method. Before describing the algorithm, we give the definition of generalized differentiability of a mapping $F : \mathbb{R}^s \to \mathbb{R}^t$ with $s,\ t \in \mathbb{N}$. The mapping F is called generalized differentiable in an open set $\mathcal{V} \subset \mathbb{R}^s$ if there exists $G_F : \mathbb{R}^s \to \mathbb{R}^{s\times t}$ such that

$$\lim_{\|\delta_{\boldsymbol{v}}\|\to 0} \frac{1}{\|\delta_{\boldsymbol{v}}\|}\|F(\boldsymbol{v}+\delta_{\boldsymbol{v}}) - F(\boldsymbol{v}) - G_F(\boldsymbol{v}+\delta_{\boldsymbol{v}})\delta_{\boldsymbol{v}}\| = 0,$$

for every $\boldsymbol{v} \in \mathcal{V}$; see e.g. [22]. This definition is equivalent to the semismoothness of locally Lipschitz maps F in [33]. Thus, we can define the semismooth Newton's method as the generalized version of Newton's method for semismooth maps. In particular, given the current iterate $\boldsymbol{u}_{\mathcal{N}}^l$, the semismooth Newton iteration is

$$G_F(\boldsymbol{u}_{\mathcal{N}}^l)\delta_{\boldsymbol{u},l} = -F^\gamma(\boldsymbol{u}_{\mathcal{N}}^l), \tag{3.2}$$

with $\delta_{\boldsymbol{u},l} = \boldsymbol{u}_{\mathcal{N}}^{l+1} - \boldsymbol{u}_{\mathcal{N}}^l$.

The generalized derivative of F^γ is given by

$$G_F(\boldsymbol{u}_{\mathcal{N}}) = \Lambda_{\mathcal{N}}^\top \mathrm{div}(\mathcal{D}^\gamma(\boldsymbol{u}_{\mathcal{N}}))^{-1}\nabla\Lambda_{\mathcal{N}} + \frac{1}{2}h(\boldsymbol{u}_{\mathcal{N}})\boldsymbol{w}^\top + \frac{1}{2}\boldsymbol{w}(h(\boldsymbol{u}_{\mathcal{N}}))^\top,$$

where $h(\boldsymbol{u}_{\mathcal{N}}) = \Lambda_{\mathcal{N}}^\top \mathrm{div}\nabla(\Lambda_{\mathcal{N}}\boldsymbol{u}_{\mathcal{N}} + \Lambda_{\mathcal{U}}\boldsymbol{z})$ and $\boldsymbol{w} \in \partial((\mathcal{D}^\gamma(\boldsymbol{u}_{\mathcal{N}}))^{-1})$, with $\partial((\mathcal{D}^\gamma(\boldsymbol{u}_{\mathcal{N}}))^{-1})$ indicates the generalized derivative of $(\mathcal{D}^\gamma(\boldsymbol{u}_{\mathcal{N}}))^{-1}$, [22]. Thus, $\boldsymbol{w}$ is given by $\boldsymbol{w} = \Lambda_{\mathcal{N}}^\top\tilde{\boldsymbol{w}}$ where

$$\tilde{\boldsymbol{w}} = \begin{cases} -\mathrm{div}(\mathcal{D}^\gamma(\boldsymbol{u}_{\mathcal{N}}))^{-3}\nabla(\Lambda_{\mathcal{N}}\boldsymbol{u}_{\mathcal{N}} + \Lambda_{\mathcal{U}}\boldsymbol{z}) & \text{if } \boldsymbol{m}(\boldsymbol{u}_{\mathcal{N}}) > \gamma \\ 0 & \text{otherwise} \end{cases}$$

and $\boldsymbol{m}(\boldsymbol{u}_{\mathcal{N}}) = |\nabla(\Lambda_{\mathcal{N}}\boldsymbol{u}_{\mathcal{N}} + \Lambda_{\mathcal{U}}\boldsymbol{z})|_2$.

A solution $\delta_{\boldsymbol{u},l}$ in (3.2) may not exist or may not be unique, since it is not ensured that G_F is positive definite. For this reason, we add a small multiple of the identity matrix to G_F,

$$G_F^\varepsilon = G_F + \varepsilon I, \tag{3.3}$$

where ε is a small positive constant. Thus, substituting G_F with G_F^ε in (3.2), the semismooth Newton iteration is given by

$$G_F^\varepsilon(\boldsymbol{u}_{\mathcal{N}}^l)\delta_{\boldsymbol{u},l} = -F^\gamma(\boldsymbol{u}_{\mathcal{N}}^l), \tag{3.4}$$

with $\delta_{\boldsymbol{u},l} = \boldsymbol{u}_{\mathcal{N}}^{l+1} - \boldsymbol{u}_{\mathcal{N}}^l$. Since the regularized matrix is positive definite and symmetric, we can solve (3.4) using the conjugate gradient method, [32].

In our numerical experiments, we have tested our implementation of the algorithm with different values of $\varepsilon \in [10^{-3}, 1]$, and we always obtained good reconstructions which suggests that our method is robust with respect to the choice of ε. In the numerical experiments reported in Section 4, we fix $\varepsilon = 0.1$.

https://doi.org/10.4208/nmtma.2017.m1613 Published online by Cambridge University Press

3.1.1. Preprocessing

The problem (2.6) is very structured and partially separable. It follows from the definition of the discrete gradient operator ∇ that a noisy pixel with a noise-free neighborhood as shown in Fig. 1 is completely independent of other noisy pixels and hence can be computed independently.

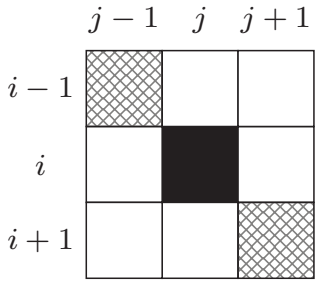


Figure 1: Neighborhood of a noisy pixel $u_{i,j}$ (black) containing six noise-free pixels (white).

Specifically, if we regard $\boldsymbol{u}$ as a matrix instead of a vector and consider a noisy pixel $u_{i,j}$ with six noise-free neighboring pixels

$$\{u_{i,j-1}, u_{i+1,j-1}, u_{i-1,j}, u_{i+1,j}, u_{i-1,j+1}, u_{i,j+1}\},$$

then it follows from (2.6) that $u_{i,j}$ can be obtained by solving an unconstrained univariate optimization problem

$$u_{i,j} = \arg\min_{v} \; H_{i,j}(v) \tag{3.5}$$

where

$$H_{i,j}(v) \;=\; \left\| \begin{pmatrix} u_{i+1,j} - v \\ u_{i,j+1} - v \end{pmatrix} \right\|_2 + \left\| \begin{pmatrix} u_{i+1,j-1} - u_{i,j-1} \\ v - u_{i,j-1} \end{pmatrix} \right\|_2 + \left\| \begin{pmatrix} v - u_{i-1,j} \\ u_{i-1,j+1} - u_{i-1,j} \end{pmatrix} \right\|_2 .$$

The function $H_{i,j}(v)$ is clearly convex, and hence the minimization problem (3.5) can be solved using e.g. the golden section search method. To this end, it is worth noticing that each of the three terms of $H_{i,j}(v)$ is coercive, and hence we can easily derive a lower bound and an upper bound on $u_{i,j}$. Indeed, the three terms of $H_{i,j}(v)$ have minimizers $(u_{i+1,j} + u_{i,j+1})/2$, $u_{i,j-1}$, and $u_{i-1,j}$, so the interval $[a, b]$ with

$$a = \min\{(u_{i+1,j} + u_{i,j+1})/2, u_{i,j-1}, u_{i-1,j}\}$$

and

$$b = \max\{(u_{i+1,j} + u_{i,j+1})/2, u_{i,j-1}, u_{i-1,j}\}$$

must contain a solution.

When the noise-level is high, there may not be many pixels with a noise-free neighborhood as shown in Fig. 1. However, it may still be possible to separate the problem

https://doi.org/10.4208/nmtma.2017.m1613 Published online by Cambridge University Press

(2.6) into a number of independent subproblems. Extraction of such subproblems can easily be automated using morphological image processing and image analysis, but in this paper, we will only consider corrupted pixels with a neighborhood as in Fig. 1 and solve for these independently.

3.1.2. Algorithm

Our denoising algorithm is summarized in Algorithm 3.1.

Algorithm 3.1. Impulse noise denoising

Detect the noise-free pixels using a noise detector.

If the estimated noise level $r \leq 30\%$, do preprocessing:

- find pixels with noise-free neighborhood;
- solve (3.5) to find optimal pixel value.

Initialize $\boldsymbol{u}_{\mathcal{N}}^0 \in \mathbb{R}^n$ as the value obtained from the previous steps and set $l = 0$.
Compute $\delta_{\boldsymbol{u},l}$, by solving the equation (3.4), and update $\boldsymbol{u}_{\mathcal{N}}^{l+1} = \boldsymbol{u}_{\mathcal{N}}^l + \delta_{\boldsymbol{u},l}$. (Note that, with preprocessing, a part of noisy pixels have been restored in step 2. In this case, the size of $\boldsymbol{u}_{\mathcal{N}}$ in (3.4) is further reduced.)
Stop if stopping criteria are satisfied; otherwise set $l = l + 1$ and go to step 4.

3.2. Solving the deblurring and denoising problem

A saddle-point formulation of the problem (2.8) is given by

$$\max_{\boldsymbol{b}\in\mathcal{B}} \min_{\boldsymbol{u}\in\mathcal{C}} \; \boldsymbol{b}^\top \nabla \boldsymbol{u}, \tag{3.6}$$

where $\boldsymbol{b} \in \mathbb{R}^{2m}$ is a dual variable, and the sets $\mathcal{C}$ and $\mathcal{B}$ are defined as

$$\mathcal{C} = \{\boldsymbol{u} \in \mathbb{R}^m \mid \Lambda_{\mathcal{U}} K \boldsymbol{u} = \Lambda_{\mathcal{U}} \boldsymbol{z}\},$$
$$\mathcal{B} = \{\boldsymbol{b} \in \mathbb{R}^{2m} \mid \|\boldsymbol{b}\|_\infty \leq 1\}.$$

The norm $\|\boldsymbol{b}\|_\infty$ denotes the discrete maximum norm, defined as

$$\|\boldsymbol{b}\|_\infty = \max_k |b_k|_2 = \max_k \sqrt{|(\boldsymbol{b}_x)_k|^2 + |(\boldsymbol{b}_y)_k|^2},$$

with

$$\boldsymbol{b} = \begin{pmatrix} \boldsymbol{b}_x \\ \boldsymbol{b}_y \end{pmatrix} \text{ and } \boldsymbol{b}_x, \boldsymbol{b}_y \in \mathbb{R}^m.$$

The Chambolle–Pock algorithm [10] for solving the convex–concave saddle-point problem (3.6) is summarized in Algorithm 3.2.

https://doi.org/10.4208/nmtma.2017.m1613 Published online by Cambridge University Press

Algorithm 3.2. Chambolle–Pock algorithm for deblurring and denoising

Detect the noise-free pixels using a noise detector.

Initialize $\boldsymbol{u}^0$ with image from step 1 and $\boldsymbol{b}^0 = \mathbf{0}$ and set $l = 0$.

Set $\theta \in [0, 1]$ and $\tau,\ \sigma > 0$ such that $\tau\sigma\|\nabla\|_2^2 < 1$.

Compute $\boldsymbol{u}^{l+1}$:

$$\boldsymbol{u}^{l+1} = P_{\mathcal{C}}(\boldsymbol{u}^l + \tau \text{div}\boldsymbol{b}^l). \tag{3.7}$$

Compute $\bar{\boldsymbol{u}}^{l+1}$:

$$\bar{\boldsymbol{u}}^{l+1} = \boldsymbol{u}^{l+1} + \theta(\boldsymbol{u}^{l+1} - \boldsymbol{u}^l). \tag{3.8}$$

Compute $\boldsymbol{b}^{l+1}$:

$$\boldsymbol{b}^{l+1} = P_{\mathcal{B}}(\boldsymbol{b}^l + \sigma\nabla\bar{\boldsymbol{u}}^{l+1}). \tag{3.9}$$

Stop if stopping criteria are satisfied; otherwise set $l = l + 1$ and go to step 4.

The projection operator $P_{\mathcal{C}}$ in (3.7) can be evaluated by solving the following least-norm problem

$$\begin{aligned} &\min_{\boldsymbol{u}} \|\boldsymbol{u} - \boldsymbol{w}^l\|_2^2 \\ &\text{s.t. } \Lambda_{\mathcal{U}} K\boldsymbol{u} = \Lambda_{\mathcal{U}}\boldsymbol{z}, \end{aligned} \tag{3.10}$$

where $\boldsymbol{w}^l = \boldsymbol{u}^l + \tau\text{div}\boldsymbol{b}^l$. This problem has the closed-form solution

$$\boldsymbol{u}^{l+1} = \boldsymbol{w}^l - K^\top\Lambda_{\mathcal{U}}^\top(\Lambda_{\mathcal{U}}KK^\top\Lambda_{\mathcal{U}}^\top)^{-1}\Lambda_{\mathcal{U}}(K\boldsymbol{w}^l - \boldsymbol{z}).$$

In order to compute the above quantity, we use the conjugate gradient method, [32]. Due to the singularity of the matrix $\Lambda_{\mathcal{U}}$, to guarantee the stability of the conjugate gradient algorithm, we add a small multiple of the identity matrix to $\Lambda_{\mathcal{U}}KK^\top\Lambda_{\mathcal{U}}^\top$.

Furthermore, the projection $P_{\mathcal{B}}$ in (3.9) is a pointwise Euclidean projection onto L^2 balls, i.e.

$$\boldsymbol{b}^{l+1} = \frac{\boldsymbol{b}^l + \sigma\nabla\bar{\boldsymbol{u}}^{l+1}}{\max(1, |\boldsymbol{b}^l + \sigma\nabla\bar{\boldsymbol{u}}^{l+1}|_2)}.$$

The Chambolle-Pock primal-dual algorithm ensures convergence if $\theta = 1$ and

$$\tau\sigma\|\nabla\|_2^2 < 1. \tag{3.11}$$

For more details we refer the reader to [10]. From [9], we know that the bound on the norm of the linear operator ∇ is

$$\|\nabla\|_2^2 = \|\text{div}\|_2^2 < 8,$$

and hence the algorithm converges if $8\tau\sigma < 1$. In our numerical experiments, we use

$$\tau = \frac{\beta}{3} \text{ and } \sigma = \frac{1}{3\beta},$$

https://doi.org/10.4208/nmtma.2017.m1613 Published online by Cambridge University Press

Table 1: PSNR values for restored images with different levels of salt-and-pepper noise given by different approaches.

	20% noise			40% noise			60% noise			80% noise		
	AM	CDH	Ours	AM	CDH	Ours	AM	CDH	Ours	AM	CDH	Ours
Boat	30.27	34.81	34.82	26.85	30.25	30.32	24.14	27.07	27.18	20.87	24.03	24.19
Bridge	28.41	32.01	32.06	25.11	28.17	28.25	22.44	25.09	25.18	19.47	22.11	22.26
Cameraman	28.66	33.60	33.59	25.27	29.14	29.13	22.59	26.23	26.29	19.97	23.07	23.14
Goldhill	29.91	34.07	34.12	27.46	30.64	30.70	24.80	27.76	27.84	22.15	25.06	25.22
Lena	32.05	36.71	36.72	28.13	32.15	32.16	24.82	28.96	28.95	21.10	25.07	25.21
Parrot	29.03	34.43	34.44	25.23	29.52	29.53	22.03	25.90	26.01	18.73	21.20	21.29
Peppers	25.47	25.58	25.60	24.44	25.26	25.27	23.02	24.67	24.68	20.25	22.91	22.96

with $\beta > 0$. In this way, the convergence of the algorithm is ensured. In our experiments described in the next section, we fixed $\beta = 0.01$ which worked well. Thus, the proposed model for deblurring and denoising is also regularization parameter-free.

4. Numerical results

In this section, we show some reconstructions obtained by applying the proposed methods to sharp and blurred images corrupted by impulse noise. For the illustrations, we use the 256×256 gray-level images: "Boat","Cameraman" and "Parrot"; see Fig. 2. The quality of the images is compared in terms of the peak signal to noise ratio (PSNR) which is defined as

$$\text{PSNR}(\boldsymbol{u}^\star) = 20 \log_{10} \frac{m|\tilde{\boldsymbol{u}}_{\max} - \tilde{\boldsymbol{u}}_{\min}|}{\|\tilde{\boldsymbol{u}} - \boldsymbol{u}^\star\|_2},$$

where $\tilde{\boldsymbol{u}}$ and $\boldsymbol{u}^\star$ represent respectively the original image and the reconstructed image with values in the gray-level range $[\tilde{\boldsymbol{u}}_{\min}, \tilde{\boldsymbol{u}}_{\max}]$. Our reconstructions are compared with the ones given by the detector (AM or ACWM) and the latest two-phase method, i.e. the one proposed in [11]. As suggested in [11], we set the parameters $\lambda = 0.0005$ and $\gamma = 0.01$ and we tune α to get the highest value of PSNR (for more details about the parameters we refer the reader to [11]). Concerning our reconstruction, based on numerical experiment, we set $\varepsilon = 0.1$ and $\gamma = 0.01$, as in the CDH method. In our simulations, we stop our algorithm as soon as there are not big changes in the iterations, i.e.,

$$\frac{\|\boldsymbol{u}^l - \boldsymbol{u}^{l-1}\|_2}{\|\boldsymbol{u}^l\|_2} < 10^{-5}.$$

In our first experiment, we consider denoising without blurring. Recall that in the first phase of our algorithm, we detect the noisy pixels using the adaptive median (AM) filter [24] for salt-and-pepper noise and the adaptive center-weighted median (ACWM) filter [16] for random-valued impulse noise. In the second phase, we solve the minimization problem (2.6) to denoise the corrupted pixels.

In Fig. 3, we show the restored images from salt-and-pepper noise using (i) the adaptive median filter [24], (ii) the CDH method [11], and (iii) our method. For

https://doi.org/10.4208/nmtma.2017.m1613 Published online by Cambridge University Press

Table 2: Comparison of CPU time (in seconds) for "Pirate" corrupted by salt-and-pepper noise.

Noise	CDH method	Our method	
		No preprocessing	Preprocessing
10%	177.9	54.7	33.7
20%	202.1	83.4	69.6
30%	199.9	110.3	101.3
40%	284.0	142.8	-
50%	293.9	195.2	-
60%	353.3	245.1	-
70%	359.3	313.0	-
80%	425.8	375.5	-



Figure 2: Original images: "Parrot", "Cameraman" and "Boat".

the CDH method, we adjusted the regularization parameter through numerical tests and show the best results. Comparing the PSNRs listed in Table 1, we see that the proposed method outperforms the AM filter and is competitive when compared to the CDH method. Taking into account that the proposed model is regularization parameter-free and only restores the noisy pixels, it is more practical and more efficient than the CDH method.

To compare the computational cost, we list the CPU time of the CDH method and the proposed method in Table 2. All of the numerical experiments were carried out in MATLAB R2014a on a PC equipped with a 3.20GHz CPU and 8GB memory. The results are based on the 1024×1024 test image "Pirate" and represent the average computation time based on ten noise realizations. Note that since the first phase of the CDH method and our method is same and the main computational load is in the second phase, we only give the CPU time associated with the second phase in Table 2. To show the effect of the preprocessing step in our method, we report the CPU times for restoration with and without the preprocessing when the noise level is at most 30%. Based on the results in Table 2, we find that the CDH method is slower than our method, especially when the noise-level is low. Moreover, the results verify that preprocessing is beneficial when the noise-level is low. Furthermore, the computation times for the CDH method do not include the overhead of tuning the regularization parameter, and hence the results do

https://doi.org/10.4208/nmtma.2017.m1613 Published online by Cambridge University Press

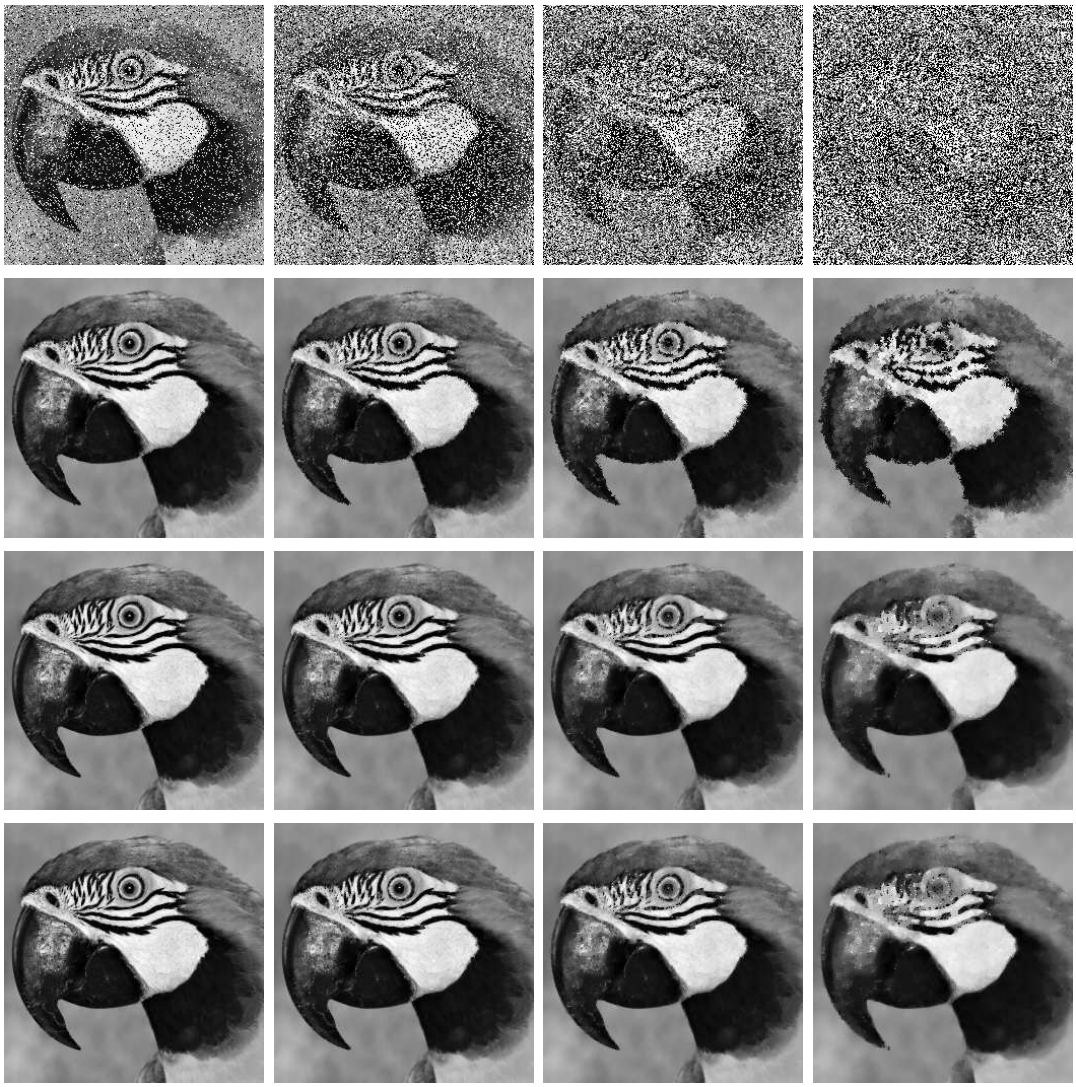


Figure 3: First row: noisy images "Parrot" with salt-and-pepper noise with noise level 20%, 40%, 60%, and 80% (left to right). Second row: results obtained with AM filter. Third row: results obtained with CDH method ($\alpha = 0.16$, $\alpha = 0.18$, $\alpha = 0.2$ and $\alpha = 0.25$). Fourth row: results obtained with proposed method.

not reflect the added advantage of our model being regularization parameter-free.

In Fig. 4, we show the results when restoring the image "Parrot" corrupted by 30% random-valued impulse noise. In the first phase, we use the ACWM filter [16] as noise detector. In case of higher noise level, others filter (see for instance [1] and [18]), which have the capability to detect noisy pixels up to 60% noise level, might be employed. From the Table 3, it is clear that our method still provides results similar to those obtained with the CDH method, and both methods outperform the ACWM filter. As for salt-and-pepper case, the main advantages are that the proposed model does not require the adjustment of the regularization parameter and, since it reconstructs only

https://doi.org/10.4208/nmtma.2017.m1613 Published online by Cambridge University Press

Table 3: PSNR values for restored images with different levels of random valued impulse noise given by different approaches.

	30% noise			40% noise		
	ACWM	CDH	Ours	ACWM	CDH	Ours
Boat	25.85	26.08	26.09	24.27	24.74	24.75
Bridge	24.17	24.61	24.61	22.57	23.18	23.19
Cameraman	24.17	24.19	24.20	22.75	23.15	23.14
Goldhill	26.68	27.04	27.02	25.02	25.73	25.75
Lena	27.13	27.01	27.03	25.01	26.16	26.16
Parrot	23.62	23.83	23.82	21.72	22.05	22.04
Peppers	26.33	26.88	26.83	24.37	25.26	25.25



Figure 4: From left to right: noisy image "Parrot" corrupted by 30% random-valued impulse noise, image restored with ACWM filter, image restored with CDH method ($\alpha = 0.15$), and image restored with proposed method.

the noisy pixels, it is faster than the CDH method.

As a final experiment, we compare the CDH method [11] and the method proposed in Section 3.2 for restoring blurred images with salt-and-pepper noise. In our simulation, we consider Gaussian blur with window size 7×7 and standard deviation 5. Fig. 5 shows the degraded images and the restored images obtained with the AM filter, the CDH method and our method. In addition, in Table 4 we list the PSNRs for different images restored with different methods. Moreover, to see how the amount of blur affects the quality of the reconstructions we test our model with Gaussian blur with window size 11×11 and standard deviation 7. The results for the image "Boat" are shown in Fig. 6. From Figs. 5 and 6, we see that the results given by the AM filter are still blurred, since there is no deblurring step in the filter. Comparing the results of the two TV-based methods, i.e. CDH and ours, we have that both methods yield good restorations. However, like the proposed denoising model, our denoising and deblurring model does not require any regularization parameters adjustment.

In Fig. 7, we compare the PSNR values for the CDH method, using different regularization parameters α in (2.1), and our method. For this purpose, we use the blurred image "Cameraman" with 40% and 60% salt-and-pepper noise (see Fig. 5 second and third column, respectively). Note that, only in the continuous case the constrained minimization problem in (2.8) is equivalent to the unconstrained minimization problem

https://doi.org/10.4208/nmtma.2017.m1613 Published online by Cambridge University Press



Figure 5: First row: Corrupted image "Cameraman" with salt-and-pepper noise with noise level 20%, 40%, 60%, and 80% and Gaussian blur with window size 7×7 and standard deviation 5. Second row: results obtained with the AM filter. Third row: results obtained with the CDH method ($\alpha = 0.0008$, $\alpha = 0.0011$, $\alpha = 0.0018$ and $\alpha = 0.0033$). Fourth row: results obtained with our method.

in (2.7), if the regularization parameter is sufficiently small (see for more details [32, Thm. 17.3]). While, in the discrete case, we can see that due to numerical issues the theorem does not hold. From the figure, it is clear that the performance of the CDH method strongly depends on the selection of α. With a value of α that differs only slightly from the best choice, the restoration results can be much worse. Hence, being regularization parameter-free, our method is much more practical and always provides comparable restored images with the CDH method.

https://doi.org/10.4208/nmtma.2017.m1613 Published online by Cambridge University Press

Table 4: PSNR values for restored blurred images with different levels of salt-and-pepper noise given by different approaches.

	20% noise			40% noise			60% noise			80% noise		
	AM	CDH	Ours	AM	CDH	Ours	AM	CDH	Ours	AM	CDH	Ours
Boat	23.00	38.85	39.00	22.90	35.78	36.02	22.68	32.13	32.09	21.88	27.74	27.79
Bridge	21.55	33.74	33.62	21.46	31.09	31.08	21.19	28.34	28.32	20.49	25.47	25.46
Cameraman	21.87	38.09	38.16	21.79	34.63	35.05	21.55	31.07	31.33	20.77	26.62	26.65
Goldhill	24.31	35.73	35.56	24.21	33.31	33.36	23.94	30.70	30.69	23.20	27.94	27.85
Lena	24.03	38.15	38.19	23.80	35.38	35.60	23.32	32.17	32.38	22.00	29.16	29.14
Parrot	21.02	37.16	37.24	20.88	33.95	34.08	20.55	30.18	30.43	19.41	26.47	26.48
Peppers	22.96	41.04	40.83	22.81	38.74	38.57	22.38	35.09	35.32	21.24	30.31	30.27



Figure 6: From the left to the right: corrupted image "Boat" with salt-and-pepper noise with noise level 40% and Gaussian blur with window size 11×11 and standard deviation 7; recovered image by using the AM filter (PSNR=21.55); recovered image by using the CDH method with $\alpha = 0.0013$ (PSNR=33.76); recovered image by using our method (PSNR=33.92).

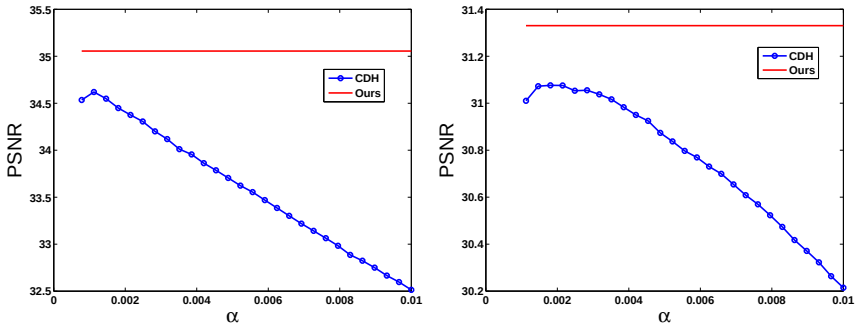


Figure 7: Comparison of the performance for the CDH method, with different values of α, and for our method for the blurred "Cameraman" with 40% and 60% salt-and-pepper noise (see Fig. 5 second and third column, respectively).

5. Conclusion

We have introduced a total-variation based regularization parameter-free model for restoring images corrupted by impulse noise. Since impulse noise only partly corrupts images, we start with a constrained minimization problem for which the CDH model [11] can be viewed as an ℓ^1-approximation of our model. In the denoising case, by separating the noisy pixels and the noise-free ones, our formulation yields an un-

https://doi.org/10.4208/nmtma.2017.m1613 Published online by Cambridge University Press

constrained problem with only the noisy pixels as variables. This reduces the size of the problem, especially for low noise-levels. We also extend our method to the simultaneous deblurring and denoising case. The main advantage of our model is that it does not require the tuning of the regularization parameter, and we have demonstrated numerically that, for the denoising case, our method provides competitive results in less time when compared to the CDH method.

Acknowledgments The work of Y. Dong is supported by Advanced Grant No. 291405 from the European Research Council.

References

[1] S. Akkoul, R. Ledee, R. Leconge, and R. Harba, *A new adaptive switching median filter*, IEEE Signal Process. Lett, 17 (2010), pp. 587–590.
[2] J. Astola and P. Kuosmanen, *Fundamentals of Nonlinear Digital Filtering*, vol. 8, CRC, Boca Raton, FL, 1997.
[3] G. Aubert and J. Aujol, *A variational approach to removing multiplicative noise*, SIAM J. Appl. Math., 68 (2008), pp. 925–946.
[4] L. Bar, N. Kiryati and N. Sochen, *Image deblurring in the presence of impulsive noise*, International Journal of Computer Vision, 70 (2006), pp. 279–298.
[5] A. Bovik, *Handbook of Image and Video Processing*, New York: Academic, 2010.
[6] D. Brownrigg, *The weighted median filter*, Comm. ACM, 27 (1984), pp. 807-818.
[7] J. Cai, R. Chan, and M. Nikolova, *Fast two-phase image deblurring under impulse noise*, J. Math. Imaging Vision, 36 (2010), pp. 46–53.
[8] J. Cai, R. Chan, and M. Nikolova, *Two-phase approach for deblurring images corrupted by impulse plus Gaussian noise*, Inverse Probl. Imaging, 2 (2008), pp. 187–204.
[9] A. Chambolle, *An algorithm for total variation minimization and applications*, J. Math. Imag. Vis., 20 (2004), pp. 89–97.
[10] A. Chambolle and T. Pock, *A first-order primal-dual algorithm for convex problems with applications to imaging*, J. Math. Imag. Vis., 40 (2011), pp. 120–145.
[11] R. Chan, Y. Dong and M. Hintermüller, *An efficient two-phase L^1- TV method for restoring blurred images with impulse noise*, IEEE Trans. Image Process., 19 (2010), pp. 1731–1739.
[12] R. Chan, C. Ho and M. Nikolova. *Salt-and-pepper noise removal by median-type noise detectors and detail-preserving regularization*, IEEE Trans. Image Process., 14 (2005), pp. 1479–1485.
[13] T. Chan and S. Esedoglu, *Aspects of total variation regularized L^1 function approximation*, SIAM J. Appl. Math., 65 (2005), pp. 1817–1837.
[14] T. Chan and J. Shen, *Image processing and analysis: variational, PDE, wavelet, and stochastic methods*, SIAM, 2005.
[15] T. Chen and H. Wu, *Space variant median filters for the restoration of impulse noise corrupted images*, IEEE Trans. Circuits Syst. II, 48 (2001), pp. 784-789.
[16] T. Chen and H. Wu, *Adaptive impulse detection using center-weighted median filters*, IEEE Signal Process. Lett., 8 (2001), pp. 1–3.
[17] Y. Dong, M. Hintermüller and M. Neri *An efficient primal dual method for L^1- TV image restoration*, SIAM J. Imag. Sci., 2 (2009), pp. 1168–1189.
[18] Y. Dong, R. Chan, and S. Xu, *A detection statistic for random-valued impulse noise*, IEEE Trans. Image Process., 16 (2007), pp. 1112-1120.

https://doi.org/10.4208/nmtma.2017.m1613 Published online by Cambridge University Press

[19] Y. Dong and T. Zeng, *A convex variational model for restoring blurred images with multiplicative noise*, SIAM J. Imaging Sci., 6 (2013), pp. 1598–1625.
[20] M. Elad and M. Aharon, *Image denoising via sparse and redundant representations over learned dictionaries*, IEEE Trans. Image Process., 15 (2006), pp. 3736–3745.
[21] B. Figueiredo and J. Bioucas-Dias, *Restoration of Poissonian images using alternating direction optimization*, IEEE Trans. Image Process., 19 (2010), pp. 3133-3145.
[22] M. Hintermüller, K. Ito and K. Kunisch, *The primal-dual active set strategy as a semismooth Newton method*, SIAM J. Opt., 13 (2002), pp. 865–888.
[23] Y. Huang, D. Lu and T. Zeng, *A Two-Step Approach for the Restoration of Images Corrupted by Multiplicative*, SIAM J. Sci. Comput., 35 (2013), pp. A2856–A2873.
[24] H. Hwang and R. Haddad *Adaptive median filters: new algorithms and results*, IEEE Trans. Image Process., 4 (1995), pp. 499–502.
[25] S. Ko and Y. Lee, *Center weighted median filters and their applications to image enhancement*, IEEE Trans. Circuits Syst., 38 (1991), pp. 984-993.
[26] T. Le, T. Chartrand, and T. Asaki, *A variational approach to reconstructing images corrupted by Poisson noise*, J. Math. Imaging Vis., 27 (2007), pp. 257–263.
[27] Y. Li, L. Shen, D. Dai and B. Suter, *Framelet algorithms for de-blurring images corrupted by impulse plus Gaussian noise*, IEEE Trans. Image Process., 20 (2011), pp. 1822-1837.
[28] L. Ma, J. Yu, and T. Zeng, *Sparse Representation Prior and Total Variation–Based Image Deblurring Under Impulse Noise*, SIAM J. Imag Sci, 6 (2013), pp. 2258-2284.
[29] L. Ma, M. Ng, J. Yu, and T. Zeng, *Efficient box-constrained TV-type-l^1 Algorithms for Restoring Images with Impulse Noise*, J. Comp. Math., 31 (2013), pp. 249–270.
[30] M. Nikolova, *Minimizers of cost-functions involving nonsmooth data-fidelity terms. Application to the processing of outliers*, SIAM J. Numer. Anal., 40 (2002), pp. 965–994.
[31] M. Nikolova, *A variational approach to remove outliers and impulse noise*, J. Math. Imag. Vis., 20 (2004), pp. 99–120, .
[32] J. Nocedal and S. Wright, *Numerical Optimization*, New York: Springer, Second edition, 2006.
[33] L. Qi and J. Sun, *A nonsmooth version of Newton's method*, Math. Programm., 58 (1993), pp 353–367.
[34] W. Pratt, *Median Filtering*, Technical report, Image Processing Institute, University of Southern California, Los Angeles, CA, 1975.
[35] L. Rudin, P. Lions, and S. Osher, *Multiplicative denoising and deblurring: theory and algorithms*, Geometric Level Sets in Imaging, Vision and Graphics, S. Osher and N. Paragios, Eds. New York: Springer, pp. 103–119, 2003.
[36] L. Rudin, S. Osher, and E. Fatemi, *Nonlinear total variation based noise removal algorithms*, Phys. D, 60 (1992), pp. 259–268.
[37] S. Setzer and G. Steidl and T. Teuber, *Deblurring Poissonian images by split Bregman techniques*, J. Visual Commun. and Image Represent., 21 (2010), pp. 193–199.
[38] Y. Xiao, T. Zeng, J. Yu and M. Ng, *Restoration of Images Corrupted by Mixed Gaussian-Impulse Noise via l_1-l_0 Minimization*, Pattern Recogn., 44 (2011), pp. 1708–1728.
[39] J. Yang, Y. Zhang and W. Yin, *An efficient TVL1 algorithm for deblurring multichannel images corrupted by impulsive noise*, SIAM J. Sci. Comput., 31 (2009), pp. 2842–2865.
[40] W. Yin, D. Goldfarb and S. Osher, *The total variation regularized L^1 model for multiscale decomposition*, Multiscale Model. Simul., 6 (2007), pp. 190–211.

https://doi.org/10.4208/nmtma.2017.m1613 Published online by Cambridge University Press